actuators

MDPI

Article

A Hybrid Control Strategy for a PMSM-Based Aircraft Cargo Door Actuator

Xin Wang *, Xiaolu Wang, Zhao Xue, Peng Guo and Shuai Liu

Beijing Institute of Precision Mechatronics and Controls, Laboratory of Aerospace Servo Actuation and Transmission (LASAT), Beijing 100076, China
* Correspondence: wxdhr0@163.com

Abstract: There are some disadvantages of a traditional AC-induced motor or hydraulic cylinder-based aircraft cargo door actuator (CDA), such as strong stopping shock, big slippage, high power, or current demand. To solve these problems, a permanent magnet synchronous motor (PMSM)-based linear CDA has been developed, and a hybrid control method combining speed plan and control, power current restriction has been proposed. In other words, low-speed-loop servo control is used in opening and closing positions, and power restricted control is adopted otherwise. A multidisciplinary model is constructed with Simulink. The simulation results show that vibration and slippage are reduced dramatically for the cargo door mechanism, and power is restricted during the whole procedure, which also results in good adaptability performance over a wide range of loads and temperatures. Experiments with different load levels on a test rig and in a temperature chamber at −50 °C are implemented to verify the effectiveness of the strategy.

Keywords: civil aircraft cargo door; PMSM-based actuator; hybrid control; power restriction

Citation: Wang, X.; Wang, X.; Xue, Z.; Guo, P.; Liu, S. A Hybrid Control Strategy for a PMSM-Based Aircraft Cargo Door Actuator. *Actuators* **2022**, *11*, 256. https://doi.org/10.3390/act11090256

Academic Editors: Ronald M. Barrett and Ignazio Dimino

Received: 28 July 2022
Accepted: 4 September 2022
Published: 8 September 2022

1. Introduction

The actuation systems on aircrafts can be classified as hydraulic actuators (HAs), electromechanical actuators (EMAs), and electro hydrostatic actuators (EHAs) according to the energy source [1]. With the development of more electric aircraft (MEA) and power-by-wire, EMAs have achieved many advantages thanks to the elimination of oil and the application of power electronics, such as lightweight and clean structure, as well as superior control and diagnostic function [1,2].

Nowadays, EMAs have become more common, and many related techniques have been applied to a variety of advanced airplanes, such as A380, B787, and many unmanned air vehicles. There are plenty of linear EMAs on airplanes, which can be used on the undercarriages, the wings, and the cargo doors. Hence, it is very important to improve the adaptability and control effect of EMAs.

Linear EMAs usually consist of a controller, motor, gear reducer, screw, and so on. There are many kinds of motors that are widely used in modern industry. As the PMSM has the advantages of high-power density and light weight, it is much more popular than asynchronous motors or DC motors in EMAs [3–5].

How to drive PMSM properly is the core problem to improve the robustness of the system. There are a lot of algorithms to control the PMSM [6], but for the PMSM in the EMA discussed in this paper, which is surface-mounted, the speed-current double vector control system based on $i_d = 0$ can approximate the maximum torque per ampere [7]. Many nonlinear intelligent controllers have been proposed with very good performance in servo systems, such as slide mode control [8], neural network control [9], fuzzy control [10], active disturbance rejection control (ADRC) [11], adaptive robust control [12], and so on. Compared to those, PID controllers are very classic and easy to realize.

The EMA discussed in this paper is installed between the cargo door and the airframe structure. The most important job of the EMA is to receive commands from the ground

crew and push or pull the door to open or close. Obviously, the starting and ending positions of the door must be precise, and the movement should be smooth. As a result, a position-speed loop is commonly used. [12] A speed loop is indispensable to make the movement process smoother. In a previous study [13], a speed planning strategy was designed in order to ensure that the door can be started or stopped steadily at any position.

To raise the efficiency of aircraft, the time of opening or closing the cargo door should be as short as possible. The actuator should work at maximum speed or power. Additionally, the equipment electrical characteristics should meet strict demands [14,15]. If the current is too high, the circuit breaker will trip to protect the whole system and cause a restart, which makes the system much less efficient. For the EMA on a cargo door, the power current protection can easily occur when the working environment is bad. In previous studies [16,17], the constant power control method by power direct control and weak magnetic field have been discussed.

In this paper, a hybrid control strategy for the cargo door actuator is proposed. By using this method, the adaptability of the actuator to load and weather is improved. The speed and power are both controlled to make the system work safely, quickly, and smoothly.

The rest of this paper is organized as follows. First, the structural and movement model of the EMA are introduced. The speed loop, power loop, and hybrid strategies for controlling the actuator are then compared. In Sections 4 and 5, the simulations and experiments are carried out to compare different control methods in different loads or temperatures. Finally, conclusions are offered in Section 6.

2. System and Load Model

2.1. System Architecture

The installation and movement of the cargo door actuator are shown schematically in Figures 1 and 2. It can be seen that the EMA is installed between the cargo door near the hinge and the airframe structure. The linear EMA is composed of a controller, PMSM, gear reducer, screw, sensors, and so on.

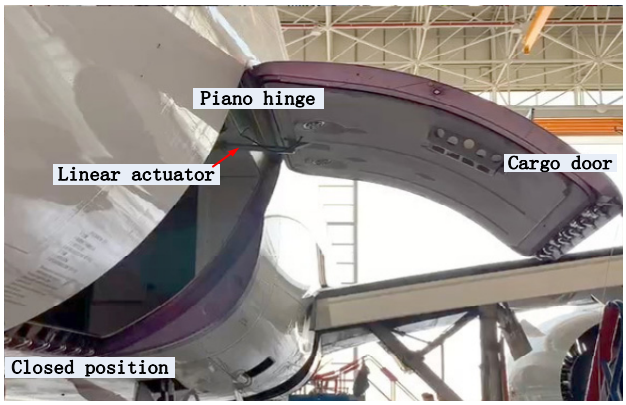

Figure 1. Installation of the cargo door actuation system.

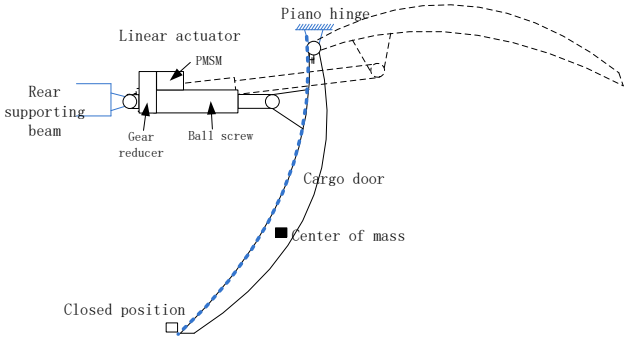

Figure 2. Function diagram of the cargo door actuation system.

The cargo door is closed when the EMA is at zero position, and it opens as the EMA stretches. Therefore, by controlling the PMSM to rotate forward or backward, we can make the cargo door open or close. The angel between the cargo door and the vector direction is [−37°,90°] from the closed position to opened position. The center of mass of the cargo door is shown in Figure 2. The EMA's load, including gravity, friction, and wind, increases as the cargo door opens [13]. The load of the EMA is shown in Figure 3. The x label is the length of the actuator, and the y label is the gravity load.

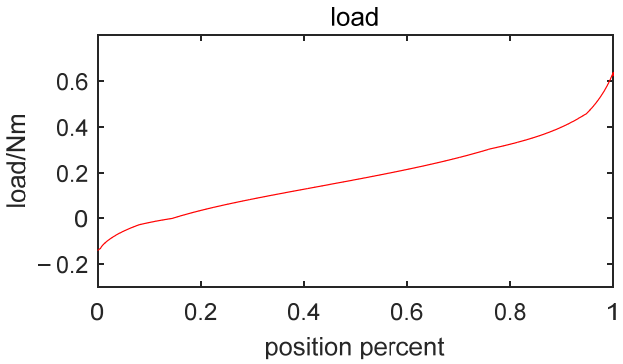

Figure 3. Load curve.

2.2. PMSM-Based EMA Model

In this paper, a speed loop and current loop with $i_d = 0$ make up the double closed-loop vector control method, which make the cargo door's movement smoother. The motion model is as follows [18]:

$$L_d = L_q \tag{1}$$

$$T_e = \frac{3}{2} p_n \psi_f i_q \tag{2}$$

$$T_e = T_l + J\frac{d\omega_r}{dt} + B\omega_r \tag{3}$$

where T_e is the electromagnetic torque, p_n is the pole pairs' number, ψ_f is the flux linkage, i_d and i_q are the stator currents on d-q axis, T_l is the load torque, J is the moment of inertia, ω_r is the mechanical angular velocity, B is the damping coefficient, and L_d and L_q are the equivalent inductances on d and q axis, respectively.

The power of PMSM can be described as follows:

$$P = UI_{dc};\ P_e = T_e\omega_r;\ P_e = \eta P \tag{4}$$

$$P = u_d i_d + u_q i_q; \tag{5}$$

where P is the output of the power supply, U is the bus voltage, I_{dc} is the power current, P_e is the electromagnetic power of the PMSM, η is the efficiency, and u_d and u_q are the stator voltages on d-q axis. The power current can be obtained as follows:

$$I_{dc} = \frac{T_e\omega_r}{U\eta} \tag{6}$$

It can be seen from Equations (3) and (6) that the power current is positively related to the load, speed, and damping coefficient. The load torque T_l is affected by gravity, wind, temperature, and so on. Obviously, a heavier cargo door and strong wind will result in a larger T_l. Also, as the weather gets colder, the viscosity of the grease used in the ball bearings and screw increases a lot. For example, the viscosity of the AeroShell Grease 7 is 10.3 at 40 °C and more than 1150 at −50 °C. As a result, a previous study [19] has shown that viscous friction torque is not negligible.

3. Control Strategy

It is expected that the door is opened or closed placidly as fast as possible, and it is not allowed to smash on the door frame when the door is closing. To meet the above expectations, the movement process, which is low speed–acceleration–high speed–deceleration–low speed–stop, should be applied to the actuator. It is known that the load of the actuator consists of gravity, wind, and friction, the majority of which is usually gravity, and the friction becomes greater at low temperatures.

3.1. Speed Curve

The reference speed is commonly given based on time. At a certain time, the actuator should work at a certain speed [13]. The reference speed curve is calculated and installed in the software and does not change with the actual working conditions. To make the actuator more efficient, a speed planning strategy is designed, in which the speed signal value is calculated considering the position percent by Equation (7). The speed signal keeps uniformly high when the load is not large, and as the load increases, the speed decreases to reduce the maximum power of the system. With the speed closed loop, the jitter of the door frame can be eliminated during starting or stopping. The variation curves of load and speed are shown in Figures 3 and 4. The x label is the position percentage over the whole open/close distance, and the y label is the speed.

$$\omega_r = \begin{cases} \sqrt{2k_1 s} & (0 \le s < S_1) \\ \omega_{max} & (S_1 \le s < S_2) \\ 2\omega_{max} - \sqrt{2k_2 s - 2k_2 S_2 - {\omega_{max}}^2} & (S_2 \le s < S_3) \\ \omega_{min} & (S_3 \le s < S_{max}) \end{cases} \tag{7}$$

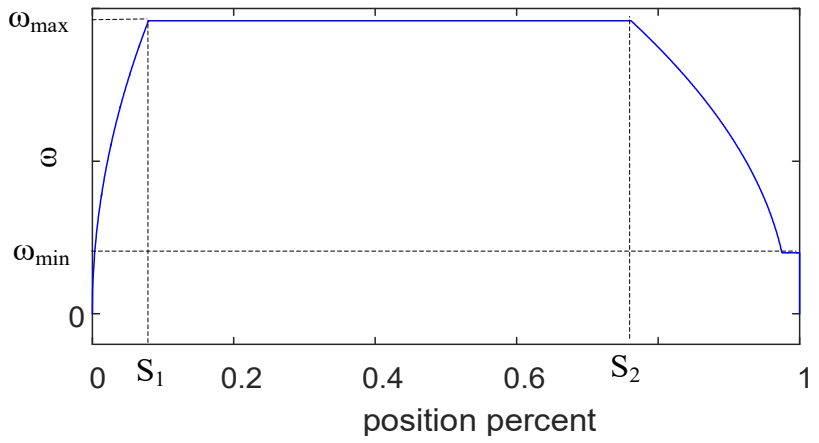

Figure 4. Speed and load curve according to the position.

3.2. Hybrid Control Strategy

By rated state, the actuator system controlled by the speed loop can work perfectly at a stable speed and low power, as planned. However, T_l may be much bigger when the wind is strong, and B may increase a lot when the temperature is low. To follow the given speed, T_e has to be bigger, as in Equation (3). If the system can track the given speed well, the system power P and power current I_{dc} have to increase, which can be seen in Equations (4) and (6).

Figure 5 shows the variation of I_{dc} with different T_l and speed. With the speed closed loop, when T_l and ${\omega_r}^*$ are large, the EMA may work in region ③, where I_{dc} is bigger than the protection threshold I_{max}, and the power will be cut off by a circuit breaker to protect the whole power system. The current protection should be avoided because it makes the cargo door stop suddenly and vibrate wildly, which is not friendly to the EMA or operator, and leads to a restart, which may waste 60 s or more.

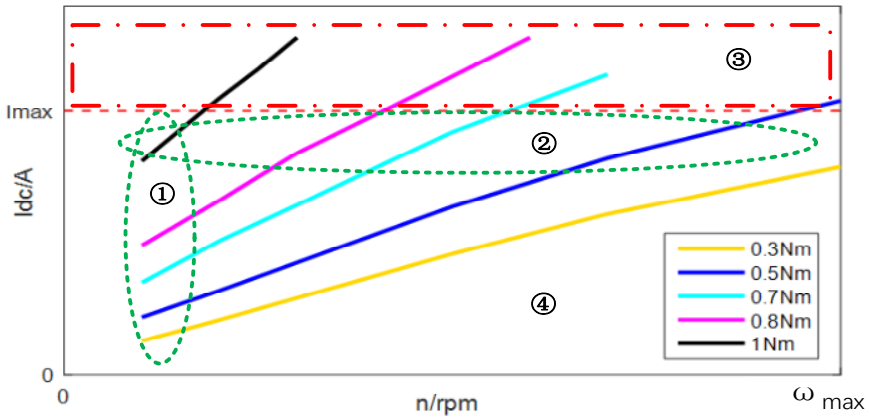

Figure 5. The variation of I_{dc} and working sections.

At the beginning and ending periods (Figure 4, $0 \leq s \leq S_1$ and $S_2 \leq s \leq S_{max}$), the speed closed loop is used, and the EMA works in region ①. In the intermediate period, if T_l is large, ${\omega_r}^*$ and I_{dc} get bigger (region ④). At a certain moment, the speed closed loop passes the handover baton to the power closed loop. The power closed loop is used to make sure that the system is working at the permitted power to safely push the cargo door (region ②).

By the use of a speed closed loop, which is commonly used to control PMSM by Equation (8), the EMA works stably with a given speed ${\omega_r}^*$ that is calculated by Equation (7). ${I_q}^*{}_2$ is the output of the speed PI controller.

$$ {I_q}^*{}_2 = K_{p2}({\omega_r}^* - \omega_r) + \int K_{i2}({\omega_r}^* - \omega_r); \tag{8} $$

The power current can be controlled by a power restricted loop, as in Equation (9), where ${I_{dc}}^*$ is the given power current, which is a little smaller than the protection threshold, and ${I_q}^*{}_1$ is the output of the power PI controller. In this way, the PMSM is dragged at the maximum permissible power.

$$ {I_q}^*{}_1 = K_{p1}({I_{dc}}^* - I_{dc}) + \int K_{i1}({I_{dc}}^* - I_{dc}); \tag{9} $$

In this paper, a control method taking advantage of the speed closed loop and power closed loop is proposed. To switch these two control methods smoothly to avoid vibration, ${I_q}^*$ is given by the smaller value of the two closed loops' outputs as follows.

$$ {I_q}^* = \min({I_q}^*{}_1,\ {I_q}^*{}_2); \tag{10} $$

At the beginning and ending periods (Figure 5-①), the speed closed loop is used, when the given speed ${\omega_r}^*$ is small and ${I_q}^*{}_2$ is small while the power current I_{dc} is little and ${I_q}^*{}_1$ is big. In the intermediate period, as ${\omega_r}^*$ and I_{dc} get bigger, ${I_q}^*{}_1$ decreases and ${I_q}^*{}_2$ increases (Figure 5-④). At a certain moment, ${I_q}^*{}_2$ passes the handover baton to ${I_q}^*{}_1$. The power closed loop is used to make sure that the system is trying its best to safely push the cargo door (Figure 5-②).

When the power closed loop actually works, it can be considered that the output of the speed closed loop is limited by the output of the power closed loop. Therefore, the core of the method is still a double closed vector control of speed and current, which makes sure that the system's stability is not changed. The control diagram is shown in Figure 6.

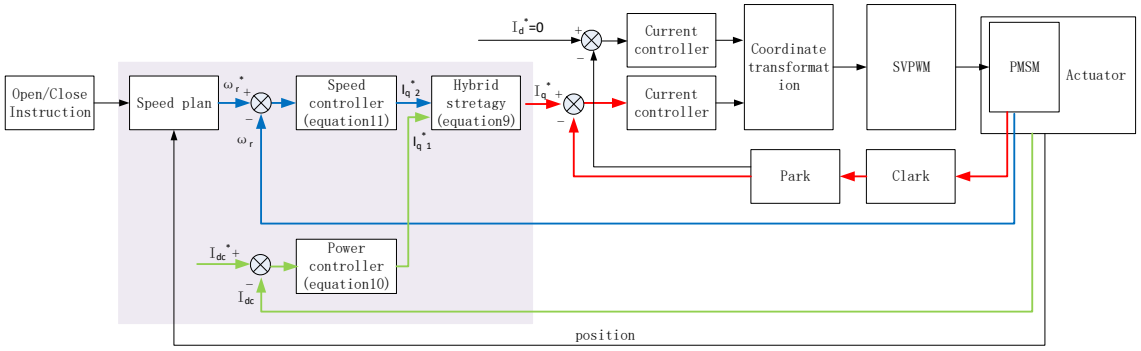

Figure 6. Block diagram of the hybrid control strategy.

4. Simulation

To verify whether the method is practicable, a simulation model was built in Simulink, which can be seen in Figure 7; the parameters are shown in Table 1.

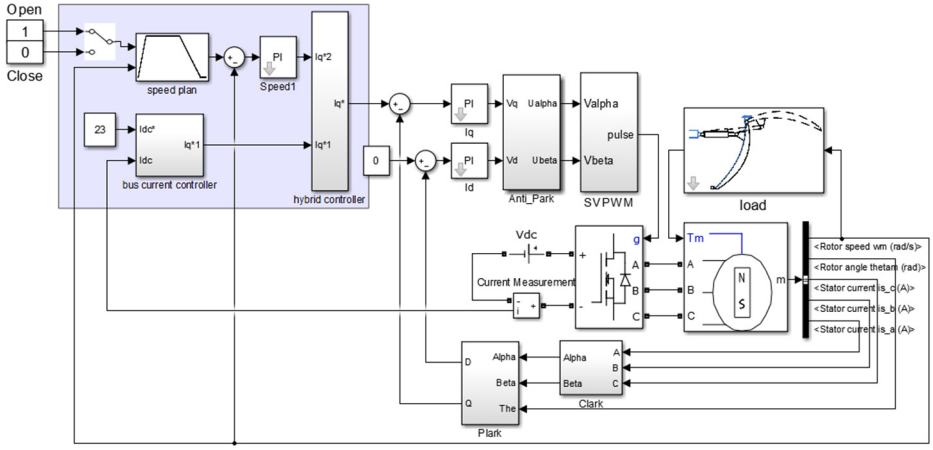

Figure 7. Diagram of the simulation model implemented in Simulink.

Table 1. Simulation parameters.

Quantity	Value	Unit
Rated power	700	W
Rated voltage	28	V
Rated torque	0.3	Nm
Rated speed	10,000	rpm
Flux linkage	0.0029	Wb
Stator resistance	0.013	Ω
d-axis or q-axis inductance	0.028×10^{-3}	mH
Pole pairs	4	
Frictional resistance coefficient	2	N · ms/rad

While the speed closed loop is the outer loop, the system's working conditions are compared when the load torque is 0.5 Nm and 1 Nm. In Figure 8a (speed), the speed of the PMSM is quite proximal to the given value, regardless of whether the load torque is large or not. When the maximum load torque is 0.5 Nm, the power current is less than 25A and the system works quite well. However, when the maximum load torque is 1 Nm, the power current will be bigger than 25A for a long time (shown in Figure 8a (I_{dc})), which is not permitted, and the system will be warned of over-current and will stop.

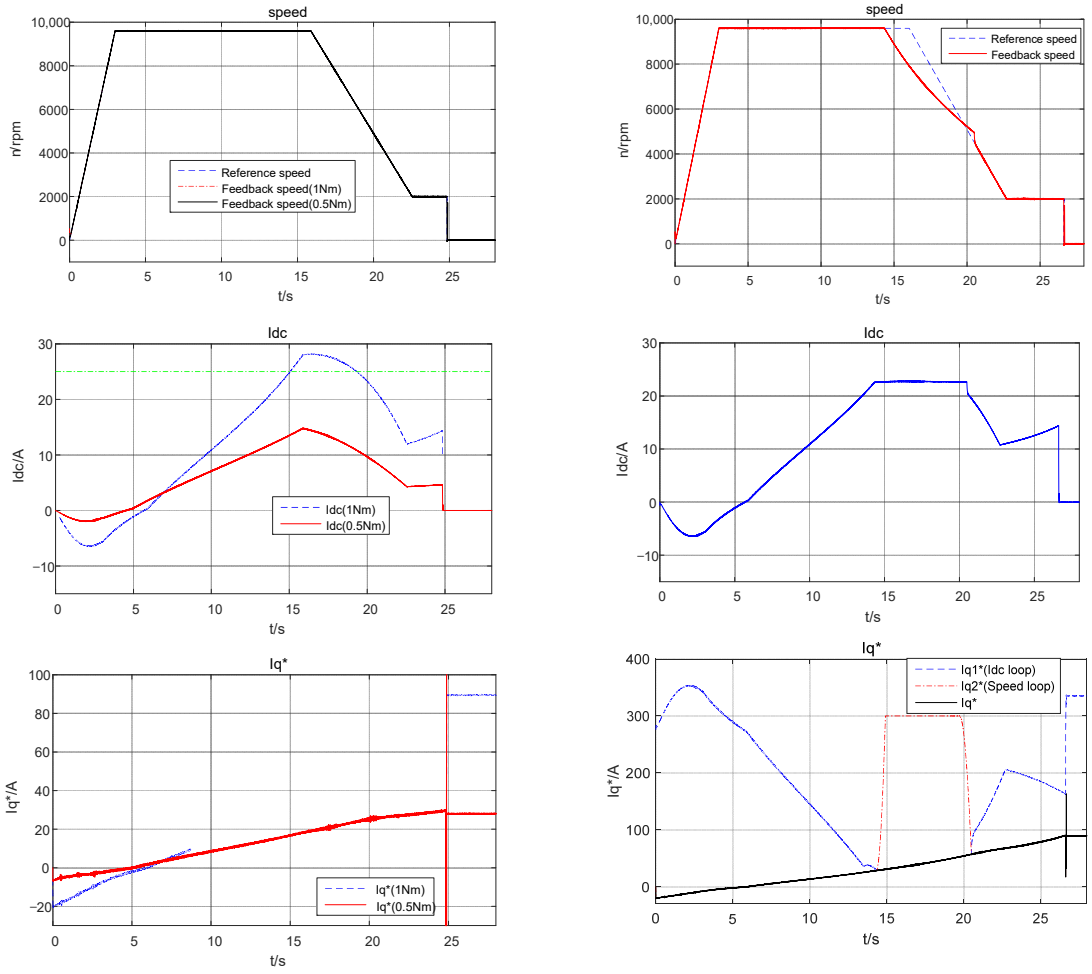

(**a**) (**b**)

Figure 8. Simulation results of speed, I_{dc}, and $I_q{}^*$. (**a**) Speed loop control when the load torque is 0.5 Nm and 1 Nm; (**b**) Hybrid control strategy when the load torque is 1 Nm.

Applying the hybrid control strategy to the system, which can be seen in Figure 8b (speed), the system slows down a little bit when the current approaches closed to the rated current (Figure 8b (I_{dc})), which means that the output of the limitation controller will be switched from the speed controller to power controller when the power current is large, and will switch back smoothly when the current is smaller (Figure 8b $(I_q{}^*)$). The system's speed is stable, and the cargo door can be opened safely and as fast as possible.

5. Experiments

There were two kinds of experiments to verify the control strategy proposed in this paper, which are shown in Figures 9–11. One was a loaded experiment and the other was a low temperature experiment, which make the EMA's load bigger by gravity and friction.

The loaded experiment was made on a gravity load test platform, which is similar to a real cargo door. By adding the adjustable steal slices on the platform, the maximum load of the PMSM was set to 1 Nm, as shown in Figure 11a. In the power closed loop, the power current $I_{dc}{}^*$ was set to 22 A. It can be seen from Figure 12a $(I_q{}^*)$ that the hybrid controller switches the $I_q{}^*$ between the output of the speed closed loop and power closed loop smoothly, the speed of the actuator slows down when the torque is getting bigger (Figure 12a (speed)), and the power current is under control (Figure 12a (I_{dc})). By applying the hybrid control strategy, the frequency of the current protection is decreased to zero. The time of the whole movement is ensured to be less than 40 s.

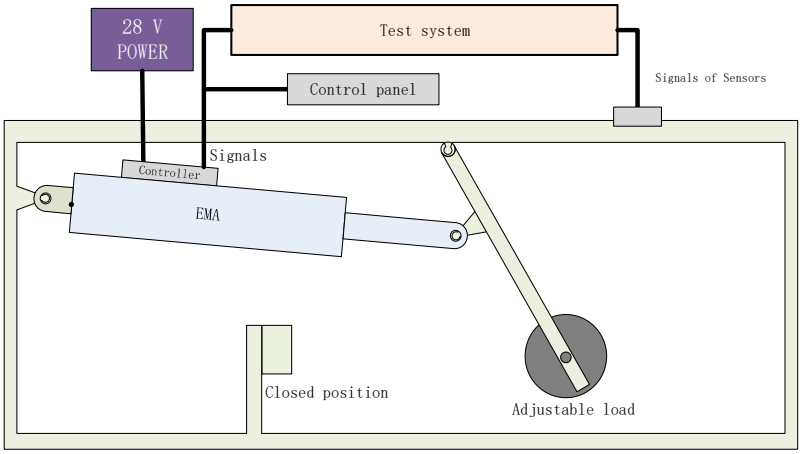

Figure 9. Block diagram of the loaded experiment.

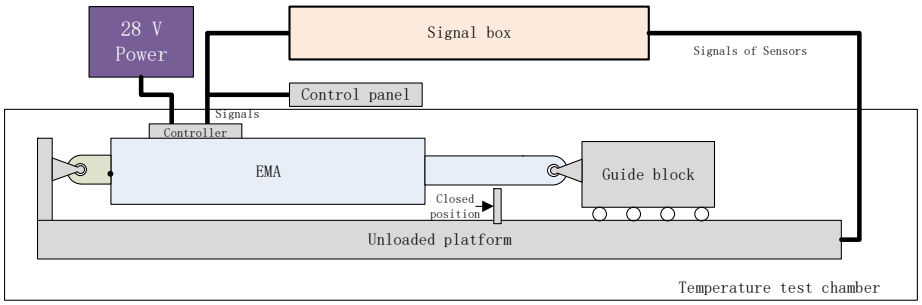

Figure 10. Block diagram of the −50 °C experiment.

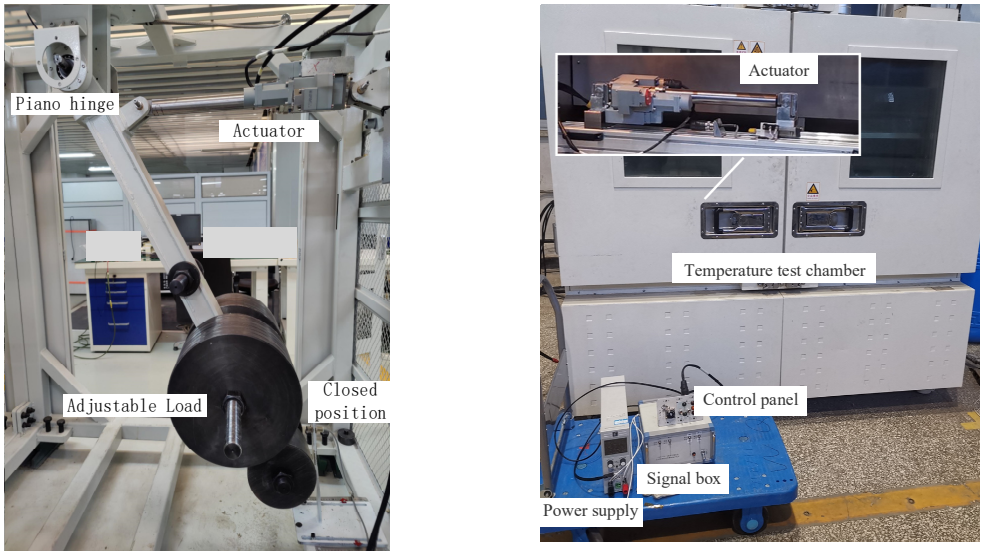

(**a**) (**b**)

Figure 11. (**a**) Actuator experiment with load at 25 °C and (**b**) without load at −50 °C.

At low temperature (−50 °C), the frictional force gets much larger because of the lubricating grease. The EMA was installed on the unloaded platform, placed in the temperature test chamber, and operated by the control panel outside the chamber, as shown in Figure 11b. The result is shown in Figure 12b. By setting the power current to a different value (17 A), the system can work efficiently too.

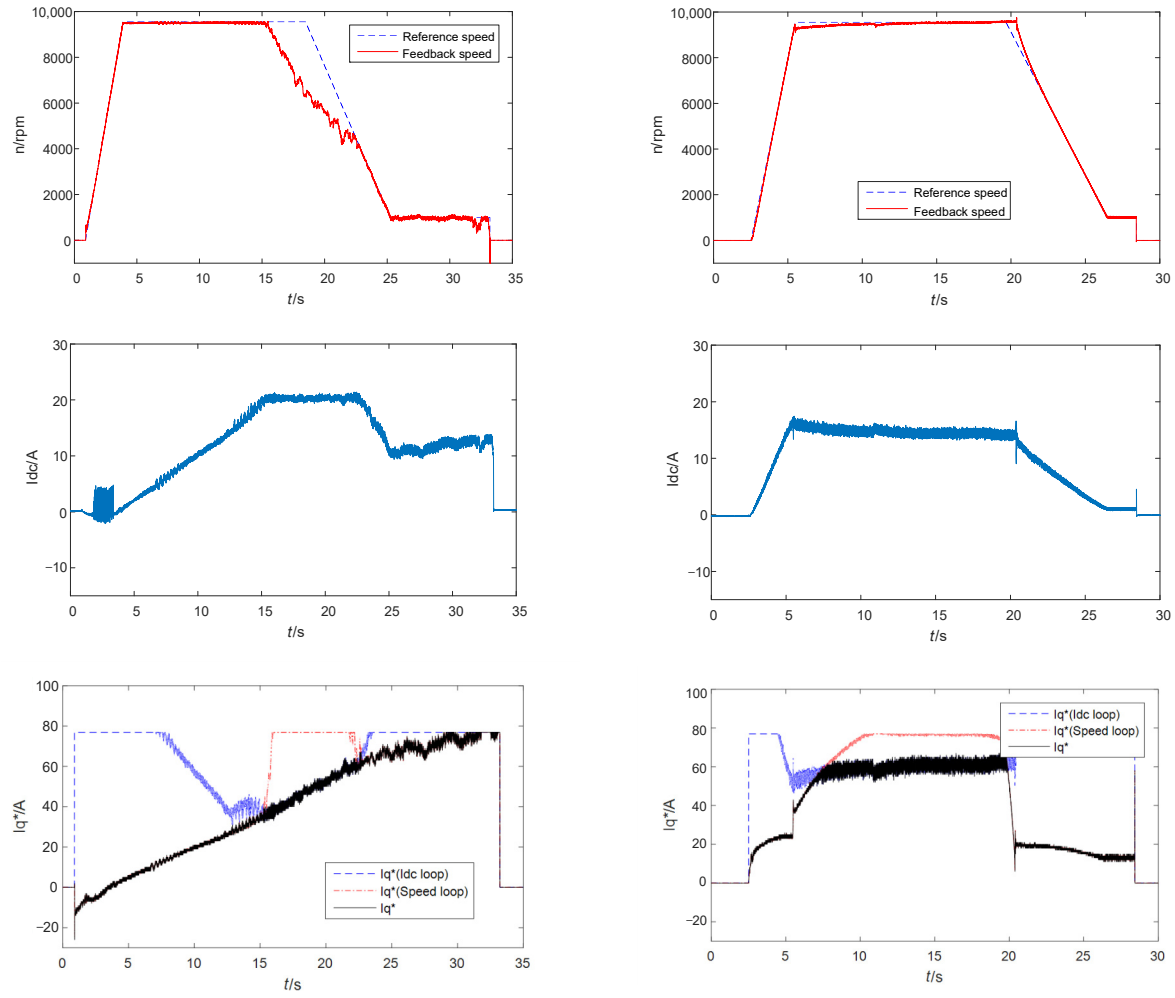

(**a**) (**b**)

Figure 12. (**a**) Speed, power current, and $I_q{}^*$ test curve with load at 25 °C and (**b**) without load at −50 °C.

6. Conclusions

In this paper, a hybrid control strategy was proposed. By combining two closed loop methods of speed and power, and switching smoothly between them, the EMA on the cargo door works much better in heavy loads and over a wide temperature range. With this approach, the actuator starts smoothly, works at its allowable maximum power and speed in the middle, and slows down and stops safely in the end. The loading capacity and adaptation to the temperature range are improved, and the over-current fault is eliminated to 0, which ensures that the whole movement takes less than 40s without current protection or restart. The hybrid control strategy was demonstrated by simulation, as well as loaded and low temperature experiments, and can be used as a reference for control systems in other fields.

Author Contributions: Conceptualization: X.W. (Xin Wang) and X.W. (Xiaolu Wang); methodology: X.W. (Xin Wang); software: Z.X.; experiments: X.W. (Xin Wang), P.G. and S.L.; formal analysis: X.W. (Xin Wang); investigation: Z.X.; resources: S.L.; data curation: X.W. (Xin Wang); writing—original draft preparation: X.W. (Xin Wang); writing—review and editing: X.W. (Xiaolu Wang); visualization: Z.X.; supervision: P.G. All authors have read and agreed to the published version of the manuscript.

Funding: This research received no external funding.

Institutional Review Board Statement: Not applicable.

Informed Consent Statement: Not applicable.

Data Availability Statement: The data presented in this study are available on request from the corresponding author.

Conflicts of Interest: The authors declare no conflict of interest.

References

1. Sayed, E.; Abdalmagid, M. Review of Electric Machines in More-/Hybrid-/Turbo-Electric Aircraft. *IEEE Trans. Transp. Electrif.* **2021**, *7*, 2976–3005. [CrossRef]
2. Giangrande, P.; Galassini, A. Considerations on the Development of an Electric Drive for a Secondary Flight Control Electromechanical Actuator. *IEEE Trans. Ind. Appl.* **2019**, *55*, 3544–3554. [CrossRef]
3. Volpato Filho, C.J.; Xiao, D.; Vieira, R.P.; Emadi, A. Observers for High-Speed Sensorless PMSM Drives: Design Methods, Tuning Challenges and Future Trends. *IEEE Access* **2021**, *9*, 56397–56415. [CrossRef]
4. Xue, Z.; Wang, Y.; Li, L.; Wang, X. An Adaptive Speed Control Method Based on Deep Reinforcement Learning for Permanent Magnet Synchronous Motor. In Proceedings of the 2021 Chinese Intelligent Systems Conference, Fuzhou, China, 16–17 October 2021.
5. Peng, W.; Lan, Y.; Chen, S.; Lin, F.; Chang, R. Reinforcement Learning Control for Six-Phase Permanent Magnet Synchronous Motor Position Servo Drive. In Proceedings of the 2020 IEEE International Conference on Knowledge Innovation and Invention (ICKII), Kaohsiung, Taiwan, 21–23 August 2020. [CrossRef]
6. Cai, W.; Wu, X. Review and Development of Electric Motor Systems and Electric Powertrains for New Energy Vehicles. *Automot. Innov.* **2021**, *4*, 3–22. [CrossRef]
7. Peng, Z. Analysis and Implementation of Constrained MTPA Criterion for Induction Machine Drives. *IEEE Access* **2020**, *8*, 176445–176453. [CrossRef]
8. Xu, W.; Junejo, A.K. An Efficient Antidisturbance Sliding-Mode Speed Control Method for PMSM Drive Systems. *IEEE Trans. Power Electron.* **2021**, *36*, 6879–6891. [CrossRef]
9. Yu, J.; Shi, P.; Dong, W.; Chen, B.; Lin, C. Neural Network-Based Adaptive Dynamic Surface Control for Permanent Magnet Synchronous Motors. *IEEE Trans. Neural Netw. Learn. Syst.* **2015**, *26*, 640–645. [CrossRef]
10. Li, S.; Gu, H. Fuzzy Adaptive Internal Model Control Schemes for PMSM Speed-Regulation System. *IEEE Trans. Ind. Inform.* **2012**, *8*, 767–779. [CrossRef]
11. Lin, P.; Wu, Z.; Liu, K.-Z.; Sun, X.-M. A Class of Linear–Nonlinear Switching Active Disturbance Rejection Speed and Current Controllers for PMSM. *IEEE Trans. Power Electron.* **2021**, *36*, 14366–14382. [CrossRef]
12. Xia, J.; Li, Z.; Yu, D.; Guo, Y.; Zhang, X. Robust Speed and Current Control with Parametric Adaptation for Surface-Mounted PMSM Considering System Perturbations. *IEEE J. Emerg. Sel. Top. Power Electron.* **2021**, *9*, 2807–2817. [CrossRef]
13. Xue, Z.; Li, L.; Wang, X.; Wei, S.; Guo, P.; Nie, Z. A motion control strategy of electro-mechanical actuator for cargo door based on FPGA. In Proceedings of the CSAA/IET International Conference on Aircraft Utility Systems, Online, 18–21 September 2020; pp. 463–468.
14. Cao, Z.; Liu, H.; Zhou, Y.; Zhang, C. Energy optimization Charateristic Analysis of More Electric Aircraft Flight Control System. In Proceedings of the 2018 IEEE 2nd International Electrical and Energy Conference (CIEEC), Beijing, China, 4–6 November 2018; pp. 227–231.
15. Alexander, R.; Meyer, D.; Wang, J. A Comparison of Electric Vehicle Power Systems to Predict Architectures, Voltage Levels, Power Requirements, and Load Characteristics of the Future All-Electric Aircraft. In Proceedings of the 2018 IEEE Transportation Electrification Conference and Expo (ITEC), Long Beach, CA, USA, 13–15 June 2018; pp. 194–200.
16. Chu, J.; Hu, Y.; Huang, W.; Li, Y.; Yang, J.; Wang, M. Direct active and reactive power control of PMSM. In Proceedings of the 2009 IEEE 6th International Power Electronics and Motion Control Conference, Wuhan, China, 17–20 May 2009; pp. 1808–1812.
17. Szenasy, I.; Varga, Z.; Szeli, Z. Optimum control strategy for PMSM in field-weakening region by constant power. In Proceedings of the 2015 International Conference on Electrical Systems for Aircraft, Railway, Ship Propulsion and Road Vehicles (ESARS), Aachen, Germany, 3–5 March 2015; pp. 1–6.
18. Bin, W.; Mehdi, N. *Control of Synchronous Motor Drive*; Wiley-IEEE Press: New York, NY, USA, 2017; pp. 353–391.
19. Jones, A.B. Ball Motion and Sliding Friction in Ball Bearings. *ASME J. Basic Eng.* **1959**, *81*, 1–12. [CrossRef]